



## Article

# Erythritol as a Saccharide Multifunctional Electrolyte Additive for Highly Reversible Zinc Anode

Linjie Li <sup>1,†</sup>, Zongwei Guo <sup>2,†</sup>, Shiteng Li <sup>3,†</sup>, Piting Cao <sup>4</sup>, Weidong Du <sup>1</sup>, Deshi Feng <sup>1</sup>, Wenhui Wei <sup>1</sup>, Fengzhao Xu <sup>1</sup>, Chuangen Ye <sup>1</sup>, Mingzhi Yang <sup>1</sup>, Jing Zhang <sup>1</sup>, Xingshuang Zhang <sup>1,\*</sup>  and Yong Li <sup>1,\*</sup> 

<sup>1</sup> Key Laboratory for High Strength Lightweight Metallic Materials of Shandong Province (HM), Advanced Materials Institute, Qilu University of Technology (Shandong Academy of Sciences), Jinan 250014, China; yangmingzhi@qlu.edu.cn (M.Y.); jzhang@sdas.org (J.Z.)

<sup>2</sup> State Key Laboratory of Biobased Materials and Green Papermaking, Qilu University of Technology (Shandong Academy of Sciences), Jinan 250353, China

<sup>3</sup> Heilongjiang Institute of Technology, College of Materials and Chemical Engineering, Harbin 150006, China

<sup>4</sup> Equipment Department, Sinopec Offshore Oilfield Service Company Shanghai Drilling Division, Shanghai 201208, China

\* Correspondence: xszhang@qlu.edu.cn (X.Z.); yongli@sdas.org (Y.L.)

† These authors contributed equally to this work.

**Abstract:** Dendrite formation and water-triggered side reactions on the surface of Zn metal anodes severely restrict the commercial viability of aqueous zinc-ion batteries (AZIBs). In this work, we introduce erythritol (Et) as an electrolyte additive to enhance the reversibility of zinc anodes, given its cost-effectiveness, mature technology, and extensive utilization in various domains such as food, medicine, and other industries. By combining multiscale theoretical simulation and experimental characterization, it was demonstrated that Et molecules can partially replace the coordination H<sub>2</sub>O molecules to reshape the Zn<sup>2+</sup> solvation sheath and destroy the hydrogen bond network of the aqueous electrolyte. More importantly, Et molecules tend to adsorb on the zinc anode surface, simultaneously inhibit water-triggered side reactions by isolating water and promote uniform and dense deposition by accelerating the Zn<sup>2+</sup> diffusion and regulating the nucleation size of the Zn grain. Thanks to this synergistic mechanism, the Zn anode can achieve a cycle life of more than 3900 h at 1 mA cm<sup>-2</sup> and an average Coulombic efficiency of 99.77%. Coupling with δ-MnO<sub>2</sub> cathodes, the full battery delivers a high specific capacity of 228.1 mAh g<sup>-1</sup> with a capacity retention of 76% over 1000 cycles at 1 A g<sup>-1</sup>.

**Keywords:** erythritol; electrolyte additive; zinc anode



**Citation:** Li, L.; Guo, Z.; Li, S.; Cao, P.; Du, W.; Feng, D.; Wei, W.; Xu, F.; Ye, C.; Yang, M.; et al. Erythritol as a Saccharide Multifunctional Electrolyte Additive for Highly Reversible Zinc Anode. *Nanomaterials* **2024**, *14*, 644. <https://doi.org/10.3390/nano14070644>

Academic Editor: Nikolaos Dimitratos

Received: 4 March 2024

Revised: 29 March 2024

Accepted: 1 April 2024

Published: 8 April 2024



**Copyright:** © 2024 by the authors. Licensee MDPI, Basel, Switzerland. This article is an open access article distributed under the terms and conditions of the Creative Commons Attribution (CC BY) license (<https://creativecommons.org/licenses/by/4.0/>).

## 1. Introduction

The development of clean energy and energy storage devices is of great significance for achieving the goal of green and sustainable development in the world [1–3]. Among various energy storage devices, lithium-ion batteries (LIBs) have been ubiquitous in every aspect of our society, including electric vehicles and consumer electronics, due to their superior energy density and cycle life [4]. However, the limited availability of lithium resources, high costs, toxic electrolytes, and safety problems hinder its further application to grid-scale energy storage systems. Fortunately, aqueous zinc-ion batteries (AZIBs) can easily circumvent these problems and have been considered a promising candidate due to being low cost, eco-friendly, and very safe [5–7]. In particular, the zinc metal anode provides a high theoretical specific capacity (820 mAh g<sup>-1</sup> or 5824 mAh cm<sup>-3</sup>), low electrochemical potential (−0.76 V vs. SHE), and good water compatibility [8]. Regrettably, the uncontrolled dendrite growth and the water-triggered side reactions on the Zn surface severely affect the reversibility of the Zn anodes, thus hindering the practical application of AZIBs [9].

So far, considerable efforts have been devoted to addressing the dendrite proliferation and the parasitic side reactions on the Zn surface [10]. Common approaches involve

coating the Zn anodes with a protective layer, designing 3D current electrode structures to facilitate deposition, employing hydrogel electrolyte or functional separators to regulate  $\text{Zn}^{2+}$  ion flux, and adding electrolyte additives to change  $\text{Zn}^{2+}$  solvation structures or modify the electrode/electrolyte interface [11,12]. In comparison, the most viable and cost-effective method is to directly use additives in aqueous electrolytes. For instance, some additives, such as dimethyl sulfoxide [13] and  $\text{Zn}(\text{H}_2\text{PO}_4)_2$  [14] can react with Zn to form a dense, stable interface layer, and inhibit dendrite growth and the side reaction by isolating the contact between active Zn and the bulk electrolyte. Some solvent additives, such as methanol [15], polyacrylamide [16], ethylene glycol [17], triethyl phosphate [18], and 15-crown-5 ether [19] can partially replace solvated water, which is conducive to restraining water-induced side reactions. Additionally, some organic molecules including supramolecular cyclodextrin [20], nettle extract [21], aromatic aldehyde [22], and arginine [23] can be adsorbed onto Zn nuclei to control the crystal plane directional growth. Furthermore, some surfactant additives such as dibenzenesulfonamide [24], perfluorooctanoic acid [25], tetrabutylammonium sulfate [26], and oleic acid [27] can bond to the Zn anode, forming a hydrophobic adsorption layer, which not only blocks the direct contact of  $\text{H}_2\text{O}$  and active Zn, thus inhibiting the side reactions, but also balances the electric field or ion distribution, thus leading to a uniform Zn deposition. However, a comprehensive evaluation of the physical/chemical properties of additives to adjust the electrolyte and the anode/electrolyte interface environment is still lacking, and the mechanism is still controversial. An efficient additive should simultaneously satisfy three characteristics: (1) It should be more nucleophilic (with a stronger Lewis alkalinity) than  $\text{H}_2\text{O}$  molecules, which can deplete the water molecules in the carrier solvation sheath, thereby reducing  $\text{H}_2\text{O}$  penetration and water-triggered side reactions. (2) It should be able to interrupt the hydrogen bond network between water molecules by forming strong hydrogen bonds with  $\text{H}_2\text{O}$  molecules, thereby reducing the mass transfer rate of  $\text{H}^+$  and  $\text{OH}^-$ . (3) It should have a small steric hindrance, which can promote the formation of a solvated sheath and improve the transport rate of charge carriers [28].

In addition, previous studies have rarely considered the price and the preparation methods of the additives because of the small amount used in AZIBs. The expensive price and the complex preparation process reduce the natural price superiority of AZIBs, especially when applied to grid-scale energy storage systems. Recently, an interesting electrolyte additive, saccharide, has attracted extensive attention due to the advantages of low cost, safety, and abundance in nature. For example, Mai's Group [29] found glucose could simultaneously modulate the solvation structure of the  $\text{Zn}^{2+}$  and Zn anode-electrolyte interface. Liang's Group [30] demonstrated that maltose could modulate solvation structures of  $\text{Zn}^{2+}$  and alleviate side reactions on Zn electrodes. Erythritol (Et) is widely found in nature, such as in fungi, melons, etc., and can also be detected in the eye lens and plasma of animals. It can be prepared by glucose fermentation, is stable at high temperatures, is stable within a wide pH range, and has been widely used in various domains such as food, medicine, and other industries.

Herein, we introduce Et as a multifunctional additive in  $\text{ZnSO}_4$ -based electrolytes and systematically reveal its regulatory mechanism for the realization of dendritic-free zinc anode. According to experimental characterization and theoretical simulation calculations, Et molecules can partially replace the coordination  $\text{H}_2\text{O}$  molecules to reshape the solvation sheath of hydrated  $\text{Zn}^{2+}$ , destroy the hydrogen bond network of the aqueous electrolyte, inhibit hydrogen evolution, and reduce the influence of side reactions. More importantly, Et molecules tend to adsorb on the zinc anode surface, not only inhibiting water-triggered side reactions by isolating water but also promoting uniform and dense deposition by accelerating the  $\text{Zn}^{2+}$  diffusion and regulating the nucleation size of the Zn grain. Thanks to this synergistic mechanism, the Zn anode can achieve a cycle life of more than 3900 h and achieve an average CE value of 99.77%. The long-cycle stability of the  $\text{Zn} \parallel \delta\text{-MnO}_2$  battery has been significantly improved, and the capacity retention rate is 76% after 1000 cycles at  $1 \text{ A g}^{-1}$ .

## 2. Results and Discussion

### 2.1. The Structure of $Zn^{2+}$ Solvation Sheath Analysis with the Et Additives

Figure 1a shows the molecular structure of Et, as a dipole molecule containing multiple hydroxyl groups, Et has stronger zinc affinity compared to  $H_2O$  molecules. It is expected to effectively regulate the structure of the  $Zn^{2+}$  solvation sheath and inhibit the activity of  $H_2O$  molecules. Firstly, the variation of the  $\nu-SO_4^{2-}$  Raman band after the addition of Et additives was investigated to explore the effect of Et molecules on the structure of the  $Zn^{2+}$  solvated sheath. According to the association between  $Zn^{2+}$  and  $SO_4^{2-}$ , there are two forms of solvation structure, solvent-separated ion pair (SSIP,  $[Zn^{2+}(H_2O)_6 \cdot SO_4^{2-}]$ ) and contact ion pair (CIP,  $[Zn^{2+}(H_2O)_5 \cdot OSO_3^{2-}]$ ). SSIP indicates a weak interaction between  $Zn^{2+}$  and  $SO_4^{2-}$ , while CIP suggests  $SO_4^{2-}$  has a strong coordination with  $Zn^{2+}$  and tends to form an inner-sphere complex [31,32]. As shown in Figure 1b, the SSIP became predominant with increasing additive concentration, while the CIP contribution gradually decreased, which indicates that  $SO_4^{2-}$  hardly affects the structure of the  $Zn^{2+}$  solvation sheath due to the strong affinity between Et molecules and  $Zn^{2+}$  [33,34]. Nuclear magnetic resonance ( $^1H$  NMR) spectra were further used to confirm the influence of Et on the  $Zn^{2+}$  solvation sheath. As shown in Figure 1c, the  $^1H$  peak of pure  $H_2O$  is located at 4.67 ppm (Figure S1, Supplementary Materials), whereas the introduction of  $ZnSO_4$  results in a noticeable increase of the chemical shift to 4.73 ppm, showing a lower electronic cloud density of  $H_2O$  due to the tight interaction between  $Zn^{2+}$  and  $H_2O$  [35]. The addition of Et will change this trend. As the dosage of Et additives increased to 2.0 g, the  $^1H$  chemical shift decreased to 4.71 ppm, indicating that the interaction between  $Zn^{2+}$  and  $H_2O$  was weakened and the coordinated  $H_2O$  molecules were dehydrated. This phenomenon is attributed to the stronger nucleophilicity of the Et molecules than the water molecules, resulting in strong coordination behavior between Et and  $Zn^{2+}$ .

Furthermore, a molecular dynamics (MD) simulation and density functional theory (DFT) calculation were carried out to analyze the evolution of the  $Zn^{2+}$  solvated sheath structure. Firstly, MD simulation was performed to investigate the  $Zn^{2+}$  solvated sheath in different electrolytes. As shown in Figure S2, the  $Zn^{2+}$  coordinates with six  $H_2O$  molecules through Zn-O bonds ( $Zn^{2+}-6H_2O$ ) in the  $ZnSO_4$  electrolyte. For the Et-containing  $ZnSO_4$  electrolyte, Et molecules rebuilt the structure of the  $Zn^{2+}$  solvate sheath by partially superseding solvated water because of the strong coordination between  $Zn^{2+}$  and Et (Figure 1d). Figure S3 shows the radial distribution function (RDF) of  $Zn^{2+}-O(Et)$  obtained from MD simulation results in the Et-containing  $ZnSO_4$  electrolyte system. The RDF of the  $Zn^{2+}-O(Et)$  bond is located at about 0.2 nm, and we calculated that the average coordination number (ACN) value of  $Zn^{2+}$  and Et was 0.399, which once again demonstrates our assumptions about the coordination mechanism. The ACN between  $Zn^{2+}$  and  $H_2O$  molecules in  $ZnSO_4$ -based electrolytes with/without Et additives was further calculated and shown in Figure 1e. The remarkable peak of the  $Zn^{2+}-O(H_2O)$  pair indicates that  $H_2O$  molecules enter into the solvation structure [36,37]. The ACN of  $Zn^{2+}-O(H_2O)$  in baseline  $ZnSO_4$  electrolyte and Et-containing electrolyte were calculated to be 5.81 and 5.41, respectively. The decreased ACN after the addition of Et additives indicates Et molecules can reshape the structure of the  $Zn^{2+}$  solvate sheath by partially superseding solvated water. The binding energies of  $[Zn(H_2O)_{6-m}(Et)_m]^{2+}$  hybrid clusters were also calculated by DFT to reveal the strong nucleophilicity of Et molecules. As shown in Figure 1f, the binding energy of  $[Zn(H_2O)_6]^{2+}$  ( $-1.799$  eV) was lower than that of  $[Zn(H_2O)_5(Et)]^{2+}$  ( $-1.968$  eV) and  $[Zn(H_2O)_4(Et)_2]^{2+}$  ( $-2.103$  eV). A higher binding energy is beneficial for additives to replace  $H_2O$  molecules from the  $[Zn(H_2O)_6]^{2+}$  clusters [38]. The binding energy of  $[Zn(H_2O)_{6-m}(Et)_m]^{2+}$  hybrid clusters increased as the Et molecules replaced more  $H_2O$  molecules within  $[Zn(H_2O)_6]^{2+}$ , further proving the superior  $Zn^{2+}$  affinity of the Et molecules.

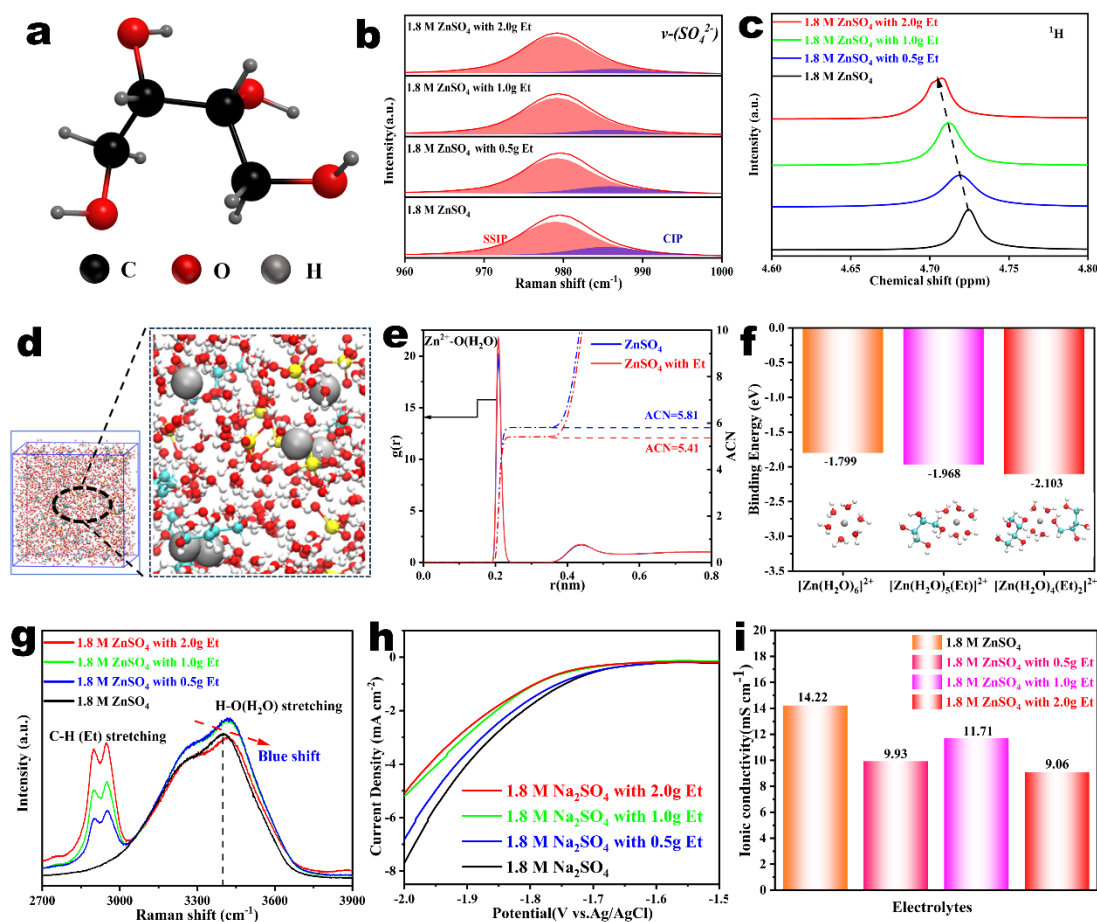


**Figure 1.** (a) Molecular structure of Et. (b) Raman spectra ( $\nu$ - $\text{SO}_4^{2-}$  band) and (c)  $^1\text{H}$  NMR of 1.8 M  $\text{ZnSO}_4$  electrolytes with various dosages of Et additives. (d) Snapshot of the MD simulation of the  $\text{ZnSO}_4$  electrolyte with Et and the local solvation structure of hydrated  $\text{Zn}^{2+}$ . (e) Average coordination number between  $\text{Zn}^{2+}$  and  $\text{H}_2\text{O}$  in the  $\text{ZnSO}_4$  electrolytes with or without Et. (f) Binding energies of original  $[\text{Zn}(\text{H}_2\text{O})_6]^{2+}$ ,  $[\text{Zn}(\text{H}_2\text{O})_5(\text{Et})]^{2+}$ , and  $[\text{Zn}(\text{H}_2\text{O})_4(\text{Et})_2]^{2+}$  hybrid cluster. (g) Raman spectra of 1.8 M  $\text{ZnSO}_4$  electrolytes with various dosages of Et. (h) Linear sweep voltammetry plots of the  $\text{Na}_2\text{SO}_4$ -based electrolytes with various dosages of Et additives. (i) The ion conductivity of 1.8 M  $\text{ZnSO}_4$  electrolytes with various dosages of Et additives.

Figure 1g shows the Raman spectra of electrolytes with different amounts of Et additive, further indicating the influence of Et. The broad characteristic peaks from 2750 to 3000  $\text{cm}^{-1}$  reflect the C-H stretching vibrations of erythritol molecules, while the O-H stretching vibrations of  $\text{H}_2\text{O}$  and erythritol molecules together facilitate a wide peak from 3000 to 3700  $\text{cm}^{-1}$ . The blue shift of the O-H peak can be observed with the addition of erythritol molecules, suggesting that the Et additives can effectively disrupt the hydrogen bond network between  $\text{H}_2\text{O}$  molecules, greatly inhibit the decomposition of water, and reduce related side reactions [39]. The polarizations in various electrolytes were monitored to estimate the inhibiting effect of Et additives on the hydrogen evolution reaction (HER). To exclude the interference of zinc plating, a  $\text{Na}_2\text{SO}_4$ -based electrolyte was used instead of the  $\text{ZnSO}_4$ -based one during linear sweep voltammetry experiments [40]. Figure 1h shows that the Et-containing electrolytes delivered a higher overpotential than the pure  $\text{Na}_2\text{SO}_4$  electrolyte. Moreover, the increase in overpotential becomes more pronounced as the concentration increases, indicating the excellent suppression effect of Et additives on the HER. Electrochemical impedance spectroscopy (EIS) was performed on various

electrolytes (Figure S4), and the corresponding ionic conductivities ( $\sigma$ ,  $\text{mS cm}^{-1}$ ) were calculated from Equation (1)

$$\sigma = \frac{z'}{z'^2 + z''^2} \cdot \frac{l}{A} \quad (1)$$

where  $A$  is the area of the Zn electrode and  $l$  is the distance between two electrodes [28,41]. Figure 1i shows that the ion conductivity of the electrolyte slightly decreases after the addition of Et additives. The ion conductivity fluctuates slightly with the increase of Et concentration. We infer that after the addition of Et, some water molecules surrounding the cation in the main solvation sheath are replaced by Et molecules, leading to an increase in free water molecules and a certain improvement in the ion conductivity of the electrolyte. Compared to the improvement in the overall performance of the battery, the loss of ionic conductivity is considered negligible. The histogram of the pH value indicates that the Et additives show almost no effect on the pH value of pure  $\text{ZnSO}_4$  electrolyte (Figure S5). Based on the above test results, it is believed that the comprehensive performance of 2 g additive concentration is the best. Next, the optimal Et additive concentration of 2 g was chosen to explore its role in stabilizing zinc metal anodes.

## 2.2. Effect of Et Additives on Deposition and Diffusion Kinetics of $\text{Zn}^{2+}$

Besides reshaping the structure of the  $\text{Zn}^{2+}$  solvation sheath, Et molecules also serve a vital role in regulating the interface environment between the zinc metal anode and electrolyte. The wettability of various electrolytes on the Zn electrode was measured by contact angles and the results are presented in Figure 2a. The Et-containing electrolyte had a smaller contact angle with zinc foil ( $71.8^\circ$ ) than that of the pure  $\text{ZnSO}_4$  electrolyte ( $86.7^\circ$ ), which suggests that the Et additives are helpful for improving the zinc affinity of the  $\text{ZnSO}_4$  electrolyte. This contributes to the uniform nucleation behavior of Zn electrodes, regulates the distribution of  $\text{Zn}^{2+}$  on the electrode surface, and has a positive impact on the stability of the electrode. To better understand the adsorption mechanism of Et, the adsorption energy of different molecules on the Zn foil was calculated using density functional theory (DFT) and illustrated in Figure 2b. The adsorption energy of the Et molecule on the Zn(002) plane ( $-0.808$  eV) was significantly larger than that of the  $\text{H}_2\text{O}$  molecule ( $-0.287$  eV). This suggests that the Et molecules can preferentially adsorb onto the zinc metal electrode and isolate active  $\text{H}_2\text{O}$  molecules from the Zn anodes, thereby reducing the parasitic side reactions and promoting uniform Zn deposition.

To better understand the mechanism by which Et regulates Zn plating, the cyclic voltammetry (CV) curve of the  $\text{Zn}^{2+}$  deposition process in different electrolytes was obtained and is shown in Figure 2c. It is evident that the nucleation over-potential after the addition of Et is larger than that of the pristine electrolyte, resulting from the different structure of the  $\text{Zn}^{2+}$  solvation sheath. The larger radius of the  $\text{Zn}^{2+}$  solvation sheath and the higher de-solvation energy during electrodeposition increase the electrochemical polarization and ultimately increase the nucleation overpotential [34]. The relationship between the Zn grain radius and the nucleation overpotential of the zinc ion obeys Formula (2)

$$r = 2 \frac{\gamma V_m}{F\eta} \quad (2)$$

where  $r$  is the radius of the  $\text{Zn}^{2+}$  nucleation,  $\gamma$  is the surface energy of the electrode/electrolyte interface,  $V_m$  is the molar volume of zinc metal,  $F$  is Faraday constant ( $96,485 \text{ C mol}^{-1}$ ), and  $\eta$  is the nucleation overpotential [42–44]. Therefore, the zinc grain radius is inversely proportional to the nucleation overpotential. The nucleation overpotential in Et-containing electrolytes increased by about 32 mV compared with pure  $\text{ZnSO}_4$  electrolyte, which means that  $\text{Zn}^{2+}$  in Et-containing electrolytes tends to form in small nuclei, thus promoting the formation of a uniform and dense deposition layer. Furthermore, the nucleation overpotential in  $\text{ZnSO}_4$ -based electrolytes with or without Et additives at various current densities were measured and shown in Figure 2d,e. The nucleation

overpotential increases with the current density, while the nucleation overpotential of the Et-containing electrolyte is higher than that of the pristine ZnSO<sub>4</sub> electrolyte under all different current densities, which echoes the above CV analysis. Chronoamperometry measurements were employed to evaluate the Zn nucleation and growth behavior in ZnSO<sub>4</sub> electrolytes with/without Et additives. For the pristine ZnSO<sub>4</sub> electrolyte, a long and chaotic in-plane diffusion process of Zn<sup>2+</sup> cations is exhibited at the initial stage, which is more conducive to the formation of Zn dendrites (Figure 2f) [36]. In contrast, the response current density for the zinc metal anode in the Et-ZnSO<sub>4</sub> electrolyte delivered a slower downtrend within the first 40 s and then stabilized. This indicates that the diffusion of Zn<sup>2+</sup> cations switches to 3D diffusion, due to the spatial confinement effect originating from the adsorption of the Et molecules on the zinc surface that shielded the 2D diffusion of the Zn<sup>2+</sup> cations.

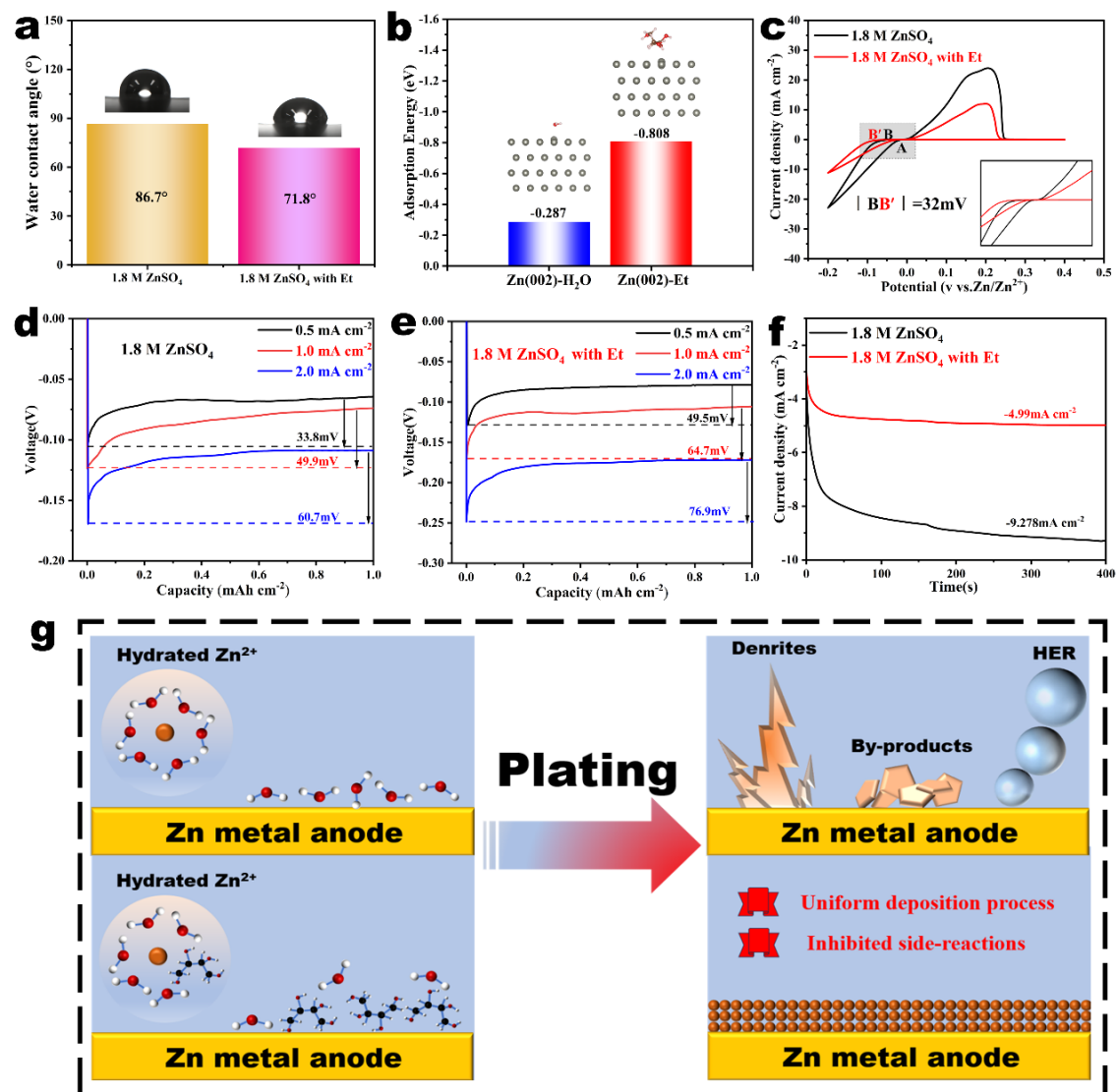


**Figure 2.** (a) Contact angles of ZnSO<sub>4</sub>-based electrolytes with/without Et on bare Zn foils. (b) The calculated adsorption energy of H<sub>2</sub>O and Et molecule on Zn(002) surface. (c) CV curves of Zn<sup>2+</sup> nucleation on Cu foil in different electrolytes. Nucleation overpotentials of Zn deposition in (d) ZnSO<sub>4</sub> electrolyte and (e) ZnSO<sub>4</sub> electrolyte with Et at different current densities. (f) Chronoamperometry curves of zinc foil in ZnSO<sub>4</sub> electrolytes with/without Et additives. (g) Schematic diagrams of zinc nucleation and growth behavior in ZnSO<sub>4</sub>-based electrolytes with and without Et additives, respectively.

According to the above experimental characterizations and theoretical calculations, we further summarized the mechanism by which Et additives improve the reversibility and stability of the zinc metal electrodes as illustrated in Figure 2g. For pristine ZnSO<sub>4</sub> electrolyte, Zn<sup>2+</sup> mainly exists in the form of [Zn(H<sub>2</sub>O)<sub>6</sub>]<sup>2+</sup>, and lots of active H<sub>2</sub>O molecules will accumulate on the zinc metal surface during the Zn plating process, which will accelerate the water-triggered side reactions and eventually lead to an inferior Coulomb efficiency (CE) and affect the reversibility of Zn electrodes. However, the Et molecules can regulate the structure of the Zn<sup>2+</sup>-solvated sheath by replacing partial H<sub>2</sub>O molecules in the solvation sheath. More importantly, the Et molecules can preferentially adsorb on the zinc anode due to the natural zincophilicity, which not only blocks the direct contact of H<sub>2</sub>O and active Zn, thus inhibiting the side reactions, but also balances the electric field or ion distribution, thus leading to a uniform Zn deposition. The above two regulatory mechanisms work together to inhibit the progression of Zn dendrite formation, hydrogen evolution corrosion, and other side reactions, and finally achieve an ultra-stable zinc anode.

### 2.3. The Impact of Et Additives on the Morphology Evolution of Zn Anodes

Anti-corrosion performance in aqueous electrolytes is another important parameter used to evaluate the stability of Zn anodes. Therefore, two Zn foils were soaked in ZnSO<sub>4</sub> electrolyte with or without Et additive for a week, respectively. As shown in Figure 3a, the zinc foil soaked in pristine ZnSO<sub>4</sub> electrolyte presented a rough surface with numerous cracks and dendrites. For comparison, the zinc foil soaked in the Et/ZnSO<sub>4</sub> hybrid electrolyte retained a smooth surface as fresh as the pristine one, confirming that the Et additives can obviously promote the corrosion resistance of Zn metal (Figure 3b). As shown in Figure 3c, the XRD patterns can confirm that the by-products appearing on the Zn electrode immersed in ZnSO<sub>4</sub> electrolyte were mainly composed of zinc hydroxide sulfate species (ZnSO<sub>4</sub>(OH)<sub>6</sub>·xH<sub>2</sub>O). The inhibition effect of Et additives on the corrosion of the Zn electrodes was also evaluated using linear polarization measurements. As exhibited by the Tafel curves (Figure 3d), compared with the Zn foil with pure ZnSO<sub>4</sub> electrolyte, the Zn foil with Et-containing electrolyte has a higher corrosion potential (−0.982 V to −0.976 V vs. Ag/AgCl) and a lower corrosion current (0.362 mA cm<sup>−2</sup> to 0.249 mA cm<sup>−2</sup>). In addition, XRD was carried out to analyze the crystal phase on the Zn anodes cycled in different electrolytes (Figure 3e). The intensity ratio between (002) and (101) of Zn electrode with pure ZnSO<sub>4</sub> electrolyte significantly decreased compared to pristine Zn after 50 cycles at a current density of 1 mA cm<sup>−2</sup>. The enhanced diffraction peak of the (101) plane suggests a longitudinal Zn deposition, which finally results in Zn dendrite growth [45]. In contrast, the Et additives clearly enhance the intensity ratio between (002) and (101), indicating that the Zn metal tends to grow parallel to the substrate, ultimately achieving a dense and uniform deposition layer. Furthermore, the intensity ratio between (002) and (101) was further increased when the current density increased to 5 mA cm<sup>−2</sup> (Figure 3f).

The surface morphology after Zn deposition in different electrolytes was further compared using SEM. Compared with the pristine zinc foil (Figure S6), the zinc foil cycled in the pristine ZnSO<sub>4</sub> electrolyte became rough and dispersed numerous flaky dendrites and by-products (Figure 3g). On the contrary, the zinc foil cycled in Et/ZnSO<sub>4</sub> hybrid electrolyte exhibited an impurity-free surface (Figure 3h). The corresponding cross-sectional SEM images also showed a dense and smooth surface for the Zn electrode cycled in Et-containing electrolyte (Figure S7). To visualize the surface morphology evolution of the zinc anode during plating, a Zn || Zn cell with a quartz inspection window was observed in real-time by in situ optical microscopy. As shown in Figure 3i, some protuberances appeared on the Zn surface of the pristine ZnSO<sub>4</sub> electrolyte after 20 min. The protuberances continuously grew and evolved into numerous Zn dendrites after 40 min. For the Et-containing electrolyte, no obvious dendrites and bubbles can be observed on the Zn surface during the plating process. The results manifest that the Et additives are beneficial to uniform Zn deposition and the corrosion resistance performance of Zn anodes, thus improving the reversibility of Zn anodes.

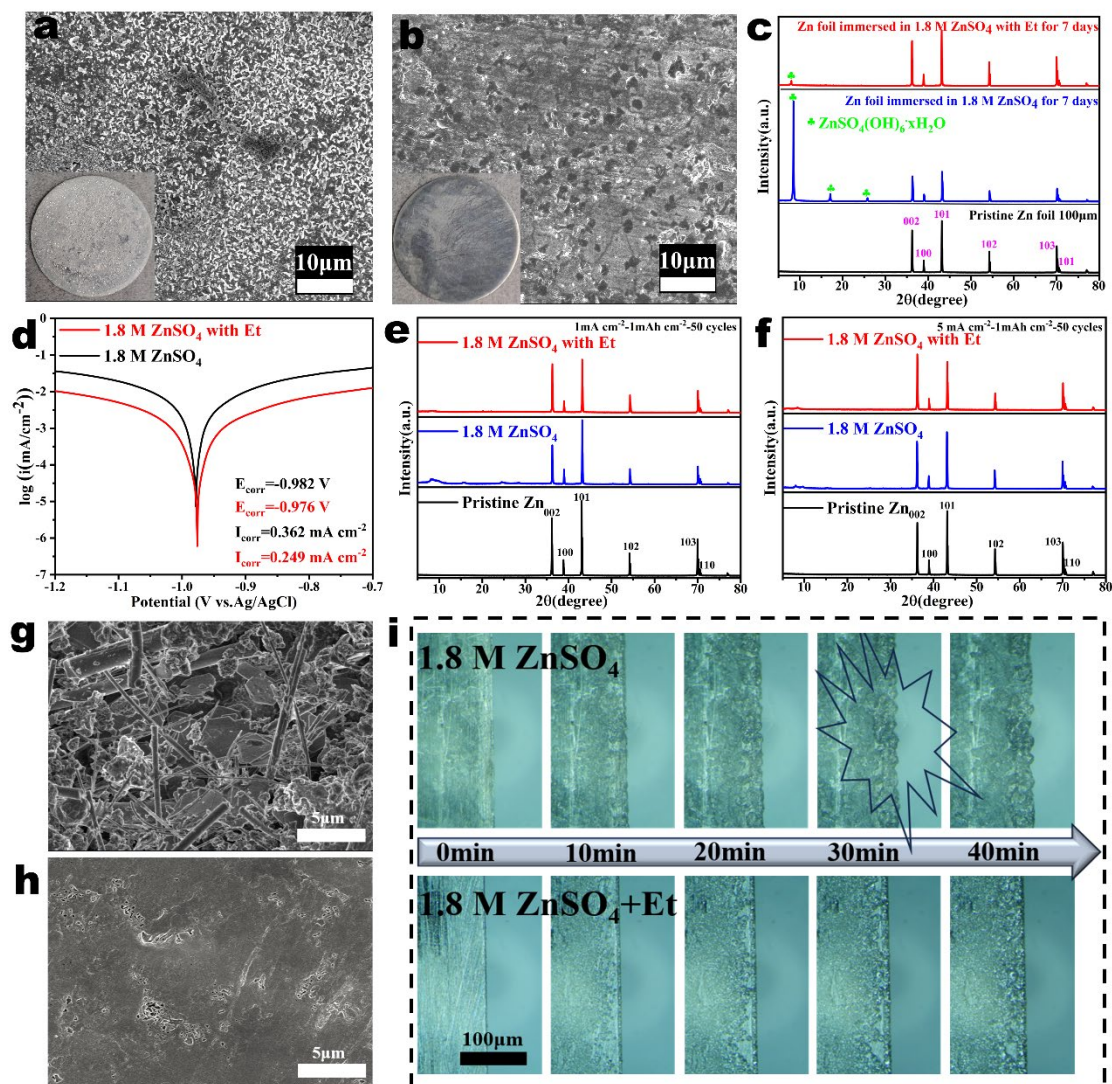


**Figure 3.** SEM images of the zinc foils after immersion in (a) the ZnSO<sub>4</sub> electrolyte and (b) the Et/ZnSO<sub>4</sub> hybrid electrolyte for a week. (c) XRD patterns of zinc foil immersed in ZnSO<sub>4</sub> electrolytes with/without Et for 7 days. (d) Tafel plots of the Zn foil at 1 mV s<sup>-1</sup> in various electrolytes based on a three-electrode system. XRD patterns of the zinc foils after 50 plating/stripping cycles in different electrolytes at different current densities: (e) 1 mA cm<sup>-2</sup> and (f) 5 mA cm<sup>-2</sup>. SEM images of the zinc foils after 50 cycles in (g) ZnSO<sub>4</sub> electrolyte and (h) the ZnSO<sub>4</sub> electrolyte with Et. (i) In situ optical observations of Zn deposition morphologies in ZnSO<sub>4</sub> electrolyte with/without Et additives.

#### 2.4. Reversibility and Stability Comparison of the Zn Anode in Various Electrolytes

To verify the positive effect of Et additives on the stability of zinc anodes, various half-cells with different electrolytes were prepared. First, the reversibility of Zn plating/stripping was evaluated using a Cu || Zn asymmetric cell. As shown in Figure 4a, the cycle life of the Zn || Cu cell is prolonged with increasing Et content at 1 mA cm<sup>-2</sup> and 1 mAh cm<sup>-2</sup>. Among them, the cell with the electrolyte containing 2 g Et provides an ultra-long cycle life of over 1500 cycles (3000 h), with an average Coulombic efficiency (CE) of 99.77%. For comparison, the CE of the cell with pristine ZnSO<sub>4</sub> electrolyte fluctuated violently after 100 plating/stripping cycles, which is caused by local short circuits resulting from severe zinc dendrites. The same trend can be observed when the current density increases to 2 mA cm<sup>-2</sup> (Figure S8). The cell with an Et-containing electrolyte operated over 1760 plating/stripping cycles (1760 h) with an average CE of 99.81%. In contrast, the cell with pristine ZnSO<sub>4</sub> electrolyte showed a higher voltage hysteresis and failed after

300 plating/stripping cycles (Figure S9). In addition, even at an ultra-high current density of  $5 \text{ mA cm}^{-2}$ , the cell with Et-containing electrolyte can remain stable over 1300 cycles (520 h), confirming the excellent reversibility of Zn anodes (Figure 4b). However, the CE of the cell with pristine  $\text{ZnSO}_4$  electrolyte showed a sharp fluctuation after 200 cycles, and the polarization increased significantly (Figure 4c,d).

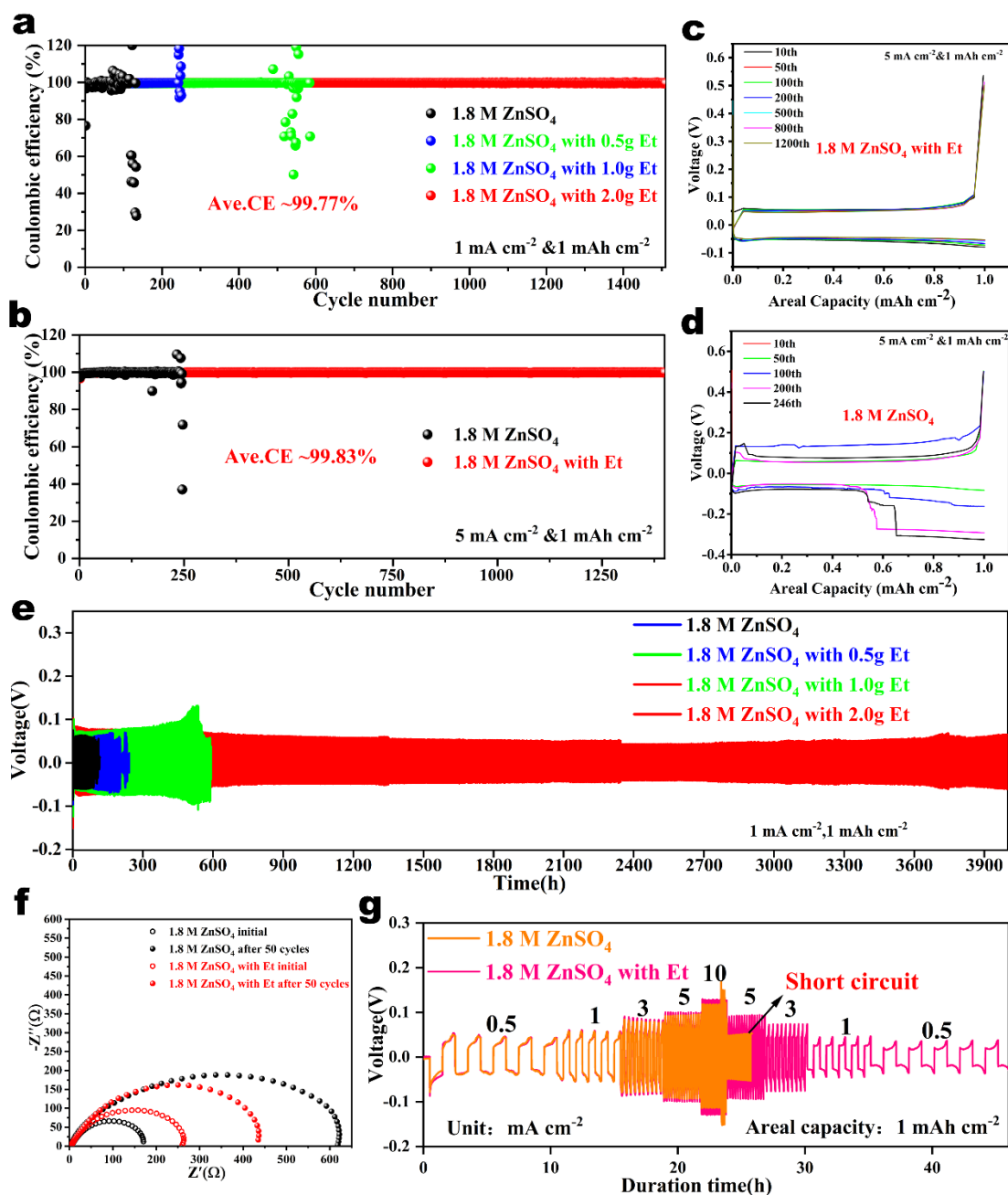


**Figure 4.** (a) CE of Zn plating/stripping at  $1 \text{ mA cm}^{-2}$  on Cu foils in  $\text{ZnSO}_4$  electrolytes with various dosages of Et additives. (b) CE of Zn plating/stripping at  $5 \text{ mA cm}^{-2}$  on Cu foils in  $\text{ZnSO}_4$  electrolytes with/without Et additives. Corresponding voltage curve diagrams of (c) with Et and (d) without Et at  $5 \text{ mA cm}^{-2}$ . (e) Cyclic stability of Zn || Zn symmetric cells in  $\text{ZnSO}_4$  electrolytes with various dosages of Et additives at  $1 \text{ mA cm}^{-2}$ . (f) The EIS results of Zn || Zn symmetric cells before and after cycling in  $\text{ZnSO}_4$  electrolytes with/without Et additives. (g) Comparison of rate capability of Zn || Zn symmetric cells in  $\text{ZnSO}_4$  electrolytes with/without Et additives.

The inhibitory effect of Et additives on dendritic growth can be further demonstrated through the long-term cycling stability of Zn | Zn symmetric cells. As shown in Figure 4e, the cycle life of the symmetric cell is prolonged with the increase of Et content at  $1 \text{ mA cm}^{-2}$  and  $1 \text{ mAh cm}^{-2}$ ; in particular, the cell with 2 g-Et/ZnSO<sub>4</sub> electrolyte has an ultra-long cycle life of over 3900 h. In contrast, the cell with pristine ZnSO<sub>4</sub> electrolyte short-circuited at about 120 h. And the same trend can be observed when the current density increases to  $5 \text{ mA cm}^{-2}$  (Figure S10). Figure 4f shows that the charge transfer impedance ( $R_{ct}$ ) of the cell with Et-containing ZnSO<sub>4</sub> electrolyte was larger than that of pristine ZnSO<sub>4</sub> electrolyte at the initial stage due to the adsorption of Et molecules on the Zn surface. Both the  $R_{ct}$  of the cells increased as the plating/stripping cycles increased, and the increase in  $R_{ct}$  was significantly smaller for the cell with an Et-containing electrolyte compared to that with pure ZnSO<sub>4</sub> electrolyte. This can be attributed to the fact that the Et-containing electrolyte can form a denser and more uniform Zn deposition layer and can effectively inhibit the generation of by-products. Furthermore, the change in thickness of the cell with an Et-containing electrolyte after cycling was smaller than that in the pristine ZnSO<sub>4</sub> electrolyte, which confirmed that the Et additives could suppress the HER (Figure S11). Figure 4g shows the rate performance of the symmetric cells in different electrolytes. As the current intensity increases from  $0.5$  to  $10 \text{ mA cm}^{-2}$ , the Zn | Zn cell with Et electrolyte showed superior cyclic reversibility, while the cell with pure ZnSO<sub>4</sub> electrolyte short-circuited rapidly. These results demonstrate that Et additives can efficiently stabilize the Zn anode at different current densities, and show superior competitiveness compared with previously reported electrolyte additives (Table S1).

### 2.5. Electrochemical Performance Comparison of AZIBs Equipped with Different Electrolytes

The Zn |  $\delta$ -MnO<sub>2</sub> full batteries with different electrolytes were assembled to evaluate the practical application of Et additives in AZIBs. The crystal phase and morphology of  $\delta$ -MnO<sub>2</sub> cathodes were characterized by XRD and SEM (Figures S12 and S13). As shown in Figure 5a, the full batteries with Et additives showed similar redox peaks to those without Et additives, confirming an analogous electrochemical response. Subsequently, the rate performance of the full batteries was tested within the range of  $0.1$  to  $5 \text{ A g}^{-1}$ . The Zn |  $\delta$ -MnO<sub>2</sub> battery utilizing Et/ZnSO<sub>4</sub> hybrid electrolyte exhibited a higher capacity compared to that in pristine ZnSO<sub>4</sub> electrolyte at various current densities (Figure 5b). The full battery with Et-containing electrolyte can still present an average capacity of  $89.7 \text{ mAh g}^{-1}$  at  $5 \text{ A g}^{-1}$ , and a high capacity of  $228.1 \text{ mAh g}^{-1}$  was achieved at  $0.1 \text{ A g}^{-1}$ . Figures 5c and S14 show the charge/discharge profiles of the batteries with or without Et additives at different rates, respectively. These results indicate that Et additives have an improved effect on the stability and durability of the entire battery system.

Figure 5d,e show the corresponding GCD curves of the batteries without or with Et additives at various cycles, respectively. The excellent cycling stability of the full batteries utilizing Et/ZnSO<sub>4</sub> hybrid electrolyte is attributed to the synergy gains of solvation and interface regulation mechanisms, which can suppress dendrite formation and water-triggered side reactions. Afterward, the cycling performance for the full batteries in different electrolytes at  $1 \text{ A g}^{-1}$  is illustrated in Figure 5f. It is worth noting that the capacity of the full battery using pristine ZnSO<sub>4</sub> electrolyte rapidly decayed to  $41.3 \text{ mAh g}^{-1}$  after 1000 cycles. For comparison, the full battery with an Et-containing electrolyte possessed a remarkable capacity ( $112.7 \text{ mA h g}^{-1}$ ) and a higher capacity retention (76%) after 1000 cycles. These results indicate that Et as an additive in ZnSO<sub>4</sub> electrolyte can effectively prolong the cycle life of zinc anodes, providing a new approach to improve the performance of aqueous zinc ion batteries.

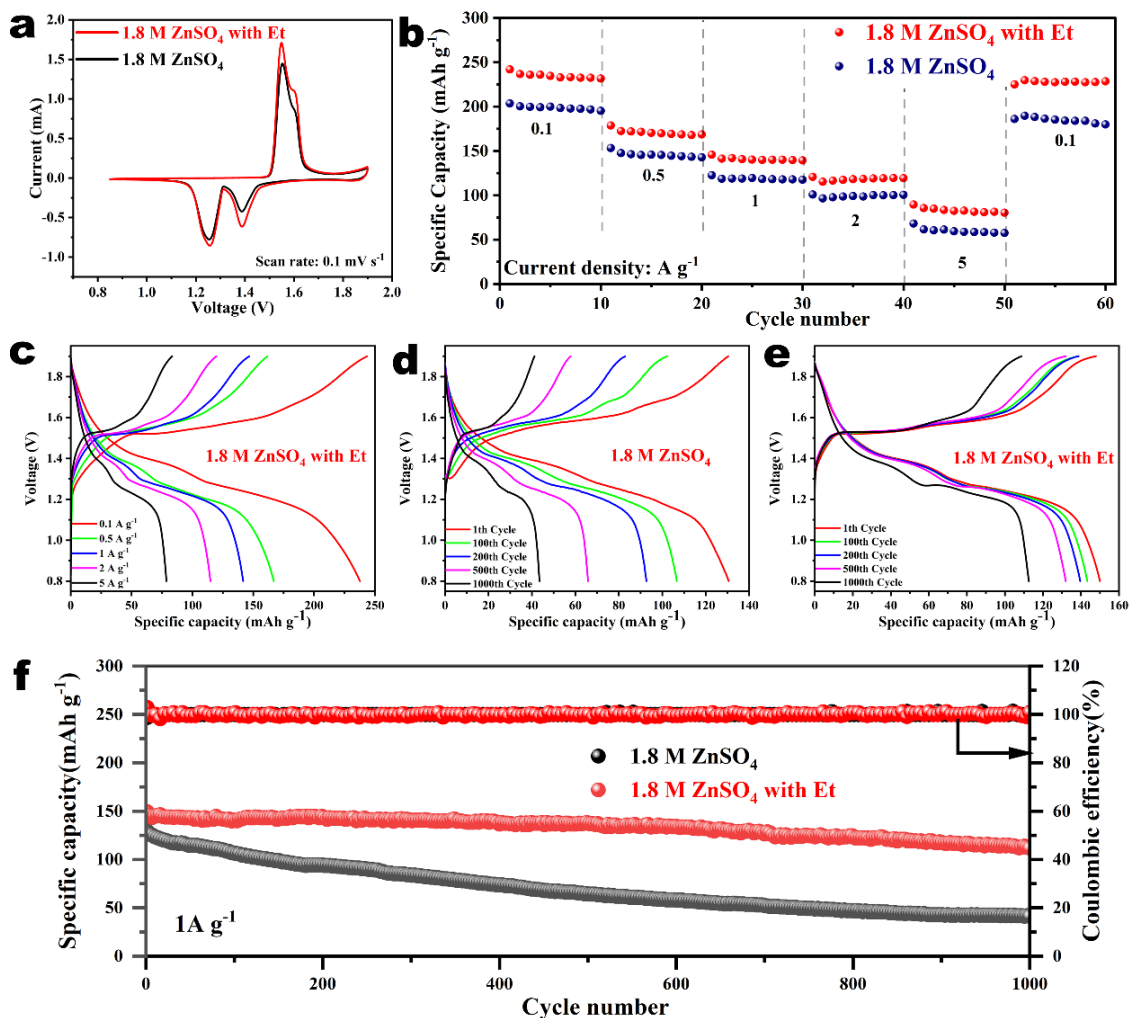


**Figure 5.** (a) CV profiles and (b) rate performance of Zn|| $\delta$ -MnO<sub>2</sub> full batteries with the electrolytes with/without Et additives. (c) Corresponding charge/discharge profiles of full battery in Et-containing electrolyte at different current densities. GCD curves of full batteries with (d) pure ZnSO<sub>4</sub> electrolyte and (e) Et-containing electrolyte at 1 A g<sup>-1</sup>. (f) Cycling performance of full batteries with different electrolytes at 1 A g<sup>-1</sup>.

### 3. Conclusions

To pursue the high reversibility of Zn metal anodes, erythritol was introduced as a multifunctional additive in ZnSO<sub>4</sub>-based electrolytes. Screening a series of electrolytes with Et shows that Et improves the cycling stability and inhibits side reactions by reshaping the environment of the electrolyte and the anode/electrolyte interface. Combined crystallographic/morphology characterizations, electrochemical analysis, DFT calculations, and MD simulation revealed that Et can reshape the Zn<sup>2+</sup> solvation structure and tends to adsorb on the zinc anode surface, isolate water, and accelerate Zn<sup>2+</sup> diffusion. The Zn||Zn symmetric cell employing an Et-containing electrolyte achieves an extremely long cycle life of more than 3900 h at 1 mA cm<sup>-2</sup> and a high CE of 99.77% over 1500 cycles. In addition, the Zn|| $\delta$ -MnO<sub>2</sub> full battery demonstrated superior cycle performance and capacity retention, providing a high capacity of 112.7 mAh g<sup>-1</sup> after 1000 cycles with a retention rate of 76%. These results show that Et additives can effectively improve the reversibility of zinc metal anodes, and the low-cost and mature preparation process of erythritol is expected to promote the application of AZIBs in grid-scale energy storage systems.

**Supplementary Materials:** The following supporting information can be downloaded at: <https://www.mdpi.com/article/10.3390/nano14070644/s1>; Figure S1. 1H NMR spectrum of pure H<sub>2</sub>O solution; Figure S2. Snapshot of the MD simulation of the ZnSO<sub>4</sub> electrolyte and the local solvation structure of hydrated Zn<sup>2+</sup>; Figure S3. RDF for Zn<sup>2+</sup>-O(Et) obtained from MD simulation results in the Et/ZnSO<sub>4</sub> hybrid electrolyte system; Figure S4. EIS of ZnSO<sub>4</sub> electrolytes with various amounts of Et and their enlarged view (inset); Figure S5. pH of ZnSO<sub>4</sub> electrolytes with various amounts of Et; Figure S6. SEM image of pristine Zn foil; Figure S7. Cross-sectional SEM images of Zn foil cycled in ZnSO<sub>4</sub> electrolyte without (a) and with (b) Et after 50 cycles; Figure S8. CE of Zn plating/stripping at 2 mA cm<sup>-2</sup> and 1 mA h cm<sup>-2</sup> on Cu foils in ZnSO<sub>4</sub>-based electrolytes with/without Et; Figure S9. The corresponding voltage curves of Zn plating/stripping at 2 mA cm<sup>-2</sup> and 1 mA h cm<sup>-2</sup> on Cu foils in ZnSO<sub>4</sub>-based electrolytes with/without Et; Figure S10. Cycling performance of the Zn||Zn cells in the different electrolytes at 5 mA cm<sup>-2</sup> and 1 mA h cm<sup>-2</sup>; Figure S11. Comparison of Zn||Zn symmetric batteries' thickness after cycling at 5 mA cm<sup>-2</sup> and 1 mA h cm<sup>-2</sup>; Figure S12. XRD pattern of the prepared δ-MnO<sub>2</sub>; Figure S13. SEM image of the prepared δ-MnO<sub>2</sub>; Figure S14. Corresponding galvanostatic charge/discharge curves of full cell with pristine 1.8 M ZnSO<sub>4</sub> electrolyte at various current densities; Table S1: Comparison of this work with previously reported electrolyte modification strategies for improving the cycling ability of Zn||Zn symmetrical cells. References [19,29,38,46–71] are also cited in the Supplementary Materials.

**Author Contributions:** Methodology, L.L., M.Y., J.Z. and Y.L.; Software, L.L., P.C., D.F., W.W., F.X. and C.Y.; Validation, L.L., Z.G., D.F., X.Z. and Y.L.; Investigation, W.D. and C.Y.; Resources, P.C.; Data curation, L.L., S.L., W.D., D.F., W.W., F.X. and C.Y.; Writing—original draft, L.L.; Writing—review & editing, X.Z. and Y.L.; Supervision, M.Y. and X.Z.; Project administration, Y.L.; Funding acquisition, M.Y., J.Z., X.Z. and Y.L. All authors have read and agreed to the published version of the manuscript.

**Funding:** This work was supported by “Youth Innovation Team Program” of Shandong Higher Education Institution (2023KJ136), National Key R&D Program of China (2019YFC1604603), National Natural Science Foundation of China (52302044, 51808328), Natural Science Foundation of Shandong Province (ZR2022QE121, ZR2023ME188, and ZR2021QE175), Innovation Pilot Project of Integration of Science, Education & Industry of Qilu University of Technology (Shandong Academy of Sciences) (2022PX-014, 2023PY055, and 2022JBZ01-07), Qilu University of Technology (Shandong Academy of Sciences), Talent Research Project (2023RCKY009).

**Data Availability Statement:** The data presented in this study are available on request from the corresponding author.

**Conflicts of Interest:** Author Piting Cao was employed by the company Equipment Department, Sinopec Offshore Oilfield Service Company Shanghai Drilling Division, Shanghai, China. The remaining authors declare that the research was conducted in the absence of any commercial or financial relationships that could be construed as a potential conflict of interest.

## References

1. Chen, S.; Zhang, M.; Zou, P.; Sun, B.; Tao, S. Historical development and novel concepts on electrolytes for aqueous rechargeable batteries. *Energy Environ. Sci.* **2022**, *15*, 1805–1839. [[CrossRef](#)]
2. Zhang, P.; Li, Y.; Wang, G.; Wang, F.; Yang, S.; Zhu, F.; Zhuang, X.; Schmidt, O.G.; Feng, X. Zn-Ion Hybrid Micro-Supercapacitors with Ultrahigh Areal Energy Density and Long-Term Durability. *Adv. Mater.* **2019**, *31*, 1806005. [[CrossRef](#)] [[PubMed](#)]
3. Nie, C.; Wang, G.; Wang, D.; Wang, M.; Gao, X.; Bai, Z.; Wang, N.; Yang, J.; Xing, Z.; Dou, S. Recent Progress on Zn Anodes for Advanced Aqueous Zinc-Ion Batteries. *Adv. Energy Mater.* **2023**, *13*, 2300606. [[CrossRef](#)]
4. Li, S.; Wang, K.; Zhang, G.; Li, S.; Xu, Y.; Zhang, X.; Zhang, X.; Zheng, S.; Sun, X.; Ma, Y. Fast Charging Anode Materials for Lithium-Ion Batteries: Current Status and Perspectives. *Adv. Funct. Mater.* **2022**, *32*, 2200796. [[CrossRef](#)]
5. Yang, H.; Zhang, T.; Chen, D.; Tan, Y.; Zhou, W.; Li, L.; Li, W.; Li, G.; Han, W.; Fan, H.; et al. Protocol in Evaluating Capacity of Zn–Mn Aqueous Batteries: A Clue of pH. *Adv. Mater.* **2023**, *35*, 2300053. [[CrossRef](#)] [[PubMed](#)]
6. Gao, X.; Yang, J.; Xu, Z.; Nuli, Y.; Wang, J. Recent progress of aqueous and organic/aqueous hybrid electrolytes for low-temperature rechargeable metal-ion batteries and supercapacitors. *Energy Storage Mater.* **2023**, *54*, 382–402. [[CrossRef](#)]
7. Yang, W.; Han, Q.; Li, W.; Wu, M.; Yao, J.; Zhao, M.; Lu, X. Ti<sub>3</sub>C<sub>2</sub>T<sub>x</sub> MXene as Janus separators for redox-enhanced electrochemical capacitors with reduced self-discharge. *Energy Storage Mater.* **2022**, *52*, 29–39. [[CrossRef](#)]
8. Cao, Z.; Zhuang, P.; Zhang, X.; Ye, M.; Shen, J.; Ajayan, P.M. Strategies for Dendrite-Free Anode in Aqueous Rechargeable Zinc Ion Batteries. *Adv. Energy Mater.* **2020**, *10*, 2001599. [[CrossRef](#)]
9. Cao, J.; Zhang, D.; Zhang, X.; Zeng, Z.; Qin, J.; Huang, Y. Strategies of regulating Zn<sup>2+</sup> solvation structures for dendrite-free and side reaction-suppressed zinc-ion batteries. *Energy Environ. Sci.* **2022**, *15*, 499–528. [[CrossRef](#)]

10. Minakshi, M. Alkaline-Earth Oxide Modified MnO<sub>2</sub> Cathode: Enhanced Performance in an Aqueous Rechargeable Battery. *Ind. Eng. Chem. Res.* **2011**, *50*, 8792–8795. [[CrossRef](#)]
11. Jiang, J.; Li, Z.; Pan, Z.; Wang, S.; Chen, Y.; Zhuang, Q.; Ju, Z.; Zhang, X. Recent Progress and Prospects on Dendrite-free Engineerings for Aqueous Zinc Metal Anodes. *Energy Environ. Mater.* **2022**, *6*, e12410. [[CrossRef](#)]
12. Guo, N.; Huo, W.; Dong, X.; Sun, Z.; Lu, Y.; Wu, X.; Dai, L.; Wang, L.; Lin, H.; Liu, H.; et al. A Review on 3D Zinc Anodes for Zinc Ion Batteries. *Small Methods* **2022**, *6*, 2200597. [[CrossRef](#)] [[PubMed](#)]
13. Cao, L.; Li, D.; Hu, E.; Xu, J.; Deng, T.; Ma, L.; Wang, Y.; Yang, X.Q.; Wang, C. Solvation Structure Design for Aqueous Zn Metal Batteries. *J. Am. Chem. Soc.* **2020**, *142*, 21404–21409. [[CrossRef](#)]
14. Zeng, X.; Mao, J.; Hao, J.; Liu, J.; Liu, S.; Wang, Z.; Wang, Y.; Zhang, S.; Zheng, T.; Liu, J.; et al. Electrolyte Design for In Situ Construction of Highly Zn<sup>2+</sup>-Conductive Solid Electrolyte Interphase to Enable High-Performance Aqueous Zn-Ion Batteries under Practical Conditions. *Adv. Mater.* **2021**, *33*, 2007416. [[CrossRef](#)] [[PubMed](#)]
15. Hao, J.; Yuan, L.; Ye, C.; Chao, D.; Davey, K.; Guo, Z.; Qiao, S. Boosting Zinc Electrode Reversibility in Aqueous Electrolytes by Using Low-Cost Antisolvents. *Angew. Chem. Int. Ed.* **2021**, *60*, 7366–7375. [[CrossRef](#)] [[PubMed](#)]
16. Zhang, Q.; Luan, J.; Fu, L.; Wu, S.; Tang, Y.; Ji, X.; Wang, H. The Three-Dimensional Dendrite-Free Zinc Anode on a Copper Mesh with a Zinc-Oriented Polyacrylamide Electrolyte Additive. *Angew. Chem. Int. Ed.* **2019**, *58*, 15841–15847. [[CrossRef](#)] [[PubMed](#)]
17. Chang, N.; Li, T.; Li, R.; Wang, S.; Yin, Y.; Zhang, H.; Li, X. An aqueous hybrid electrolyte for low-temperature zinc-based energy storage devices. *Energy Environ. Sci.* **2020**, *13*, 3527–3535. [[CrossRef](#)]
18. Liu, S.; Mao, J.; Pang, W.; Vongsvivut, J.; Zeng, X.; Thomsen, L.; Wang, Y.; Liu, J.; Li, D.; Guo, Z. Tuning the Electrolyte Solvation Structure to Suppress Cathode Dissolution, Water Reactivity, and Zn Dendrite Growth in Zinc-Ion Batteries. *Adv. Funct. Mater.* **2021**, *31*, 2104281. [[CrossRef](#)]
19. Xin, T.; Zhou, R.; Xu, Q.; Yuan, X.; Zheng, Z.; Li, Y.; Zhang, Q.; Liu, J. 15-Crown-5 ether as efficient electrolyte additive for performance enhancement of aqueous Zn-ion batteries. *Chem. Eng. J.* **2023**, *452*, 139572. [[CrossRef](#)]
20. Wang, G.; Dou, Q.; Xiong, P.; Liu, Q.; Min, D.; Park, H.S. Surface-preferred crystal plane induced by supramolecular cyclodextrin additive for highly reversible aqueous zinc metal batteries. *Chem. Eng. J.* **2023**, *457*, 141250. [[CrossRef](#)]
21. Zhang, L.; Miao, L.; Xin, W.; Peng, H.; Yan, Z.; Zhu, Z. Engineering zincophilic sites on Zn surface via plant extract additives for dendrite-free Zn anode. *Energy Storage Mater.* **2022**, *44*, 408–415. [[CrossRef](#)]
22. Qiu, M.; Ma, L.; Sun, P.; Wang, Z.; Cui, G.; Mai, W. Manipulating Interfacial Stability Via Absorption-Competition Mechanism for Long-Lifespan Zn Anode. *Nano-Micro Lett.* **2021**, *14*, 31. [[CrossRef](#)] [[PubMed](#)]
23. Lu, H.; Zhang, X.; Luo, M.; Cao, K.; Lu, Y.; Xu, B.B.; Pan, H.; Tao, K.; Jiang, Y. Amino Acid-Induced Interface Charge Engineering Enables Highly Reversible Zn Anode. *Adv. Funct. Mater.* **2021**, *31*, 2103514. [[CrossRef](#)]
24. Song, Y.; Wang, J.; Zhong, X.; Wang, K.; Zhang, Y.; Liu, H.; Zhang, L.; Liang, J.; Wen, R. Interfacial chemistry regulation via dibenzenesulfonamide-functionalized additives enables high-performance Zn metal anodes. *Energy Storage Mater.* **2023**, *58*, 85–93. [[CrossRef](#)]
25. Zhao, F.; Jing, Z.; Guo, X.; Li, J.; Dong, H.; Tan, Y.; Liu, L.; Zhou, Y.; Owen, R.; Shearing, P.R.; et al. Trace amounts of fluorinated surfactant additives enable high performance zinc-ion batteries. *Energy Storage Mater.* **2022**, *53*, 638–645. [[CrossRef](#)]
26. Bayaguud, A.; Luo, X.; Fu, Y.; Zhu, C. Cationic Surfactant-Type Electrolyte Additive Enables Three-Dimensional Dendrite-Free Zinc Anode for Stable Zinc-Ion Batteries. *ACS Energy Lett.* **2020**, *5*, 3012–3020. [[CrossRef](#)]
27. Wang, M.; Wu, X.; Yang, D.; Zhao, H.; He, L.; Su, J.; Zhang, X.; Yin, X.; Zhao, K.; Wang, Y.; et al. A colloidal aqueous electrolyte modulated by oleic acid for durable zinc metal anode. *Chem. Eng. J.* **2023**, *451*, 138589. [[CrossRef](#)]
28. Huang, Z.; Wang, T.; Li, X.; Cui, H.; Liang, G.; Yang, Q.; Chen, Z.; Chen, A.; Guo, Y.; Fan, J.; et al. Small-Dipole-Molecule-Containing Electrolytes for High-Voltage Aqueous Rechargeable Batteries. *Adv. Mater.* **2022**, *34*, 2106180. [[CrossRef](#)] [[PubMed](#)]
29. Sun, P.; Ma, L.; Zhou, W.; Qiu, M.; Wang, Z.; Chao, D.; Mai, W. Simultaneous Regulation on Solvation Shell and Electrode Interface for Dendrite-Free Zn Ion Batteries Achieved by a Low-Cost Glucose Additive. *Angew. Chem. Int. Ed.* **2021**, *60*, 18247–18255. [[CrossRef](#)]
30. Chen, W.; Guo, S.; Qin, L.; Li, L.; Cao, X.; Zhou, J.; Luo, Z.; Fang, G.; Liang, S. Hydrogen Bond-Functionalized Massive Solvation Modules Stabilizing Bilateral Interfaces. *Adv. Funct. Mater.* **2022**, *32*, 2112609. [[CrossRef](#)]
31. Rudolph, W.W.; Brooker, M.H.; Tremaine, P.R. Raman Spectroscopy of Aqueous ZnSO<sub>4</sub> Solutions under Hydrothermal Conditions: Solubility, Hydrolysis, and Sulfate Ion Pairing. *J. Solut. Chem.* **1999**, *28*, 621–630. [[CrossRef](#)]
32. Luo, M.; Wang, C.; Lu, H.; Lu, Y.; Xu, B.; Sun, W.; Pan, H.; Yan, M.; Jiang, Y. Dendrite-free zinc anode enabled by zinc-chelating chemistry. *Energy Storage Mater.* **2021**, *41*, 515–521. [[CrossRef](#)]
33. Yang, H.; Chang, Z.; Qiao, Y.; Deng, H.; Mu, X.; He, P.; Zhou, H. Constructing a Super-Saturated Electrolyte Front Surface for Stable Rechargeable Aqueous Zinc Batteries. *Angew. Chem. Int. Ed.* **2020**, *59*, 9377–9381. [[CrossRef](#)] [[PubMed](#)]
34. Yu, Y.; Zhang, P.; Wang, W.; Liu, J. Tuning the Electrode/Electrolyte Interface Enabled by a Trifunctional Inorganic Oligomer Electrolyte Additive for Highly Stable and High-Rate Zn Anodes. *Small Methods* **2023**, *7*, 2300546. [[CrossRef](#)] [[PubMed](#)]
35. Wang, B.; Zheng, R.; Yang, W.; Han, X.; Hou, C.; Zhang, Q.; Li, Y.; Li, K.; Wang, H. Synergistic Solvation and Interface Regulations of Eco-Friendly Silk Peptide Additive Enabling Stable Aqueous Zinc-Ion Batteries. *Adv. Funct. Mater.* **2022**, *32*, 2112693. [[CrossRef](#)]
36. Xu, J.; Lv, W.; Yang, W.; Jin, Y.; Jin, Q.; Sun, B.; Zhang, Z.; Wang, T.; Zheng, L.; Shi, X.; et al. In Situ Construction of Protective Films on Zn Metal Anodes via Natural Protein Additives Enabling High-Performance Zinc Ion Batteries. *ACS Nano* **2022**, *16*, 11392–11404. [[CrossRef](#)] [[PubMed](#)]

37. Xu, R.; Zhou, J.; Gong, H.; Qiao, L.; Li, Y.; Li, D.; Gao, M.; Xu, G.; Wang, M.; Liang, X.; et al. Environment-friendly degradable zinc-ion battery based on guar gum-cellulose aerogel electrolyte. *Biomater. Sci.* **2022**, *10*, 1476–1485. [[CrossRef](#)]
38. Qin, R.; Wang, Y.; Zhang, M.; Wang, Y.; Ding, S.; Song, A.; Yi, H.; Yang, L.; Song, Y.; Cui, Y.; et al. Tuning Zn<sup>2+</sup> coordination environment to suppress dendrite formation for high-performance Zn-ion batteries. *Nano Energy* **2021**, *80*, 105478. [[CrossRef](#)]
39. Zhang, S.; Li, Q.; Luo, K.; Zhong, L.; Xiong, Y.; Li, G.; Zhong, S.; Yan, D. Erythritol-strengthen electrolytes effectively improve the electrochemical stability window of aqueous symmetric supercapacitor. *Mater. Lett.* **2023**, *343*, 134384. [[CrossRef](#)]
40. Zhao, K.; Fan, G.; Liu, J.; Liu, F.; Li, J.; Zhou, X.; Ni, Y.; Yu, M.; Zhang, Y.; Su, H.; et al. Boosting the Kinetics and Stability of Zn Anodes in Aqueous Electrolytes with Supramolecular Cyclodextrin Additives. *J. Am. Chem. Soc.* **2022**, *144*, 11129–11137. [[CrossRef](#)]
41. Yang, Q.; Huang, Z.; Li, X.; Liu, Z.; Li, H.; Liang, G.; Wang, D.; Huang, Q.; Zhang, S.; Chen, S.; et al. A Wholly Degradable, Rechargeable Zn-Ti<sub>3</sub>C<sub>2</sub> MXene Capacitor with Superior Anti-Self-Discharge Function. *ACS Nano* **2019**, *13*, 8275–8283. [[CrossRef](#)] [[PubMed](#)]
42. Zhou, J.; Zhang, R.; Xu, R.; Li, Y.; Tian, W.; Gao, M.; Wang, M.; Li, D.; Liang, X.; Xie, L.; et al. Super-Assembled Hierarchical Cellulose Aerogel-Gelatin Solid Electrolyte for Implantable and Biodegradable Zinc Ion Battery. *Adv. Funct. Mater.* **2022**, *21*, 2111406. [[CrossRef](#)]
43. Zhou, J.; Li, Y.; Xie, L.; Xu, R.; Zhang, R.; Gao, M.; Tian, W.; Li, D.; Qiao, L.; Wang, T.; et al. Humidity-sensitive, shape-controllable, and transient zinc-ion batteries based on plasticizing gelatin-silk protein electrolytes. *Mater. Today Energy* **2021**, *21*, 100712. [[CrossRef](#)]
44. Huang, C.; Zhao, X.; Liu, S.; Hao, Y.; Tang, Q.; Hu, A.; Liu, Z.; Chen, X. Stabilizing Zinc Anodes by Regulating the Electrical Double Layer with Saccharin Anions. *Adv. Mater.* **2021**, *33*, 2100445. [[CrossRef](#)] [[PubMed](#)]
45. Wang, T.; Sun, J.; Hua, Y.; Krishna, B.N.V.; Xi, Q.; Ai, W.; Yu, J.S. Planar and dendrite-free zinc deposition enabled by exposed crystal plane optimization of zinc anode. *Energy Storage Mater.* **2022**, *53*, 273–304. [[CrossRef](#)]
46. Petersson, G.A.; Al-Laham, M.A. A complete basis set model chemistry. II. Open-shell systems and the total energies of the first-row atoms. *J. Chem. Phys.* **1991**, *94*, 6081–6090. [[CrossRef](#)]
47. Jorgensen, W.L.; Maxwell, D.S.; Tirado-Rives, J. Development and Testing of the OPLS All-Atom Force Field on Conformational Energetics and Properties of Organic Liquids. *J. Am. Chem. Soc.* **1996**, *118*, 11225–11236. [[CrossRef](#)]
48. Ribeiro, A.A.S.T.; Horta, B.A.C.; Alencastro, R.B.D. MKTOP: A program for automatic construction of molecular topologies. *J. Braz. Chem. Soc.* **2008**, *19*, 1433–1435. [[CrossRef](#)]
49. Van Der Spoel, D.; Lindahl, E.; Hess, B.; Groenhof, G.; Mark, A.E.; Berendsen, H.J. GROMACS: Fast, flexible, and free. *J. Comput. Chem.* **2005**, *26*, 1701–1718. [[CrossRef](#)]
50. Abraham, M.J.; Murtola, T.; Schulz, R.; Páll, S.; Smith, J.C.; Hess, B.; Lindahl, E. GROMACS: High performance molecular simulations through multi-level parallelism from laptops to supercomputers. *SoftwareX* **2015**, *1*, 19–25. [[CrossRef](#)]
51. Berendsen, H.J.C.; van der Spoel, D.; Drunen, R.V. GROMACS: A message-passing parallel molecular dynamics implementation. *Comput. Phys. Commun.* **1995**, *91*, 43–56. [[CrossRef](#)]
52. Van Gunsteren, W.F.; Berendsen, H.J.C. A Leap-frog Algorithm for Stochastic Dynamics. *Mol. Simul.* **1988**, *1*, 173–185. [[CrossRef](#)]
53. Hess, B.; Bekker, H.; Berendsen, H.J.C.; Fraaije, J.G.E.M. LINCS: A linear constraint solver for molecular simulations. *J. Comput. Chem.* **1997**, *18*, 1463–1472. [[CrossRef](#)]
54. Darden, T.; York, D.; Pedersen, L. Particle mesh Ewald: An N·log(N) method for Ewald sums in large systems. *J. Chem. Phys.* **1993**, *98*, 10089–10092. [[CrossRef](#)]
55. Kresse, G.; Furthmüller, J. Efficiency of ab-initio total energy calculations for metals and semiconductors using a plane-wave basis set. *Comput. Mater. Sci.* **1996**, *6*, 15–50. [[CrossRef](#)]
56. Kresse, G.; Furthmüller, J. Efficient Iterative Schemes for Ab Initio Total-Energy Calculations Using a Plane-Wave Basis Set. *Phys. Rev. B* **1996**, *54*, 11169–11186. [[CrossRef](#)] [[PubMed](#)]
57. Perdew, J.P.; Burke, K.; Ernzerhof, M. Generalized Gradient Approximation Made Simple. *Phys. Rev. Lett.* **1996**, *77*, 3865–3868. [[CrossRef](#)] [[PubMed](#)]
58. Kresse, G.; Joubert, D. From ultrasoft pseudopotentials to the projector augmented-wave method. *Phys. Rev. B* **1999**, *59*, 1758–1775. [[CrossRef](#)]
59. Blöchl, P.E. Projector augmented-wave method. *Phys. Rev. B* **1994**, *50*, 17953–17979. [[CrossRef](#)]
60. Monkhorst, H.J.; Pack, J.D. Special points for Brillouin-zone integrations. *Phys. Rev. B* **1976**, *13*, 5188–5192. [[CrossRef](#)]
61. Grimme, S.; Antony, J.; Ehrlich, S.; Krieg, H. A consistent and accurate ab initio parametrization of density functional dispersion correction (DFT-D) for the 94 elements H-Pu. *J. Chem. Phys.* **2010**, *132*, 154104. [[CrossRef](#)] [[PubMed](#)]
62. Grimme, S.; Ehrlich, S.; Goerigk, L. Effect of the damping function in dispersion corrected density functional theory. *J. Comput. Chem.* **2011**, *32*, 1456–1465. [[CrossRef](#)] [[PubMed](#)]
63. Hou, Z.; Tan, H.; Gao, Y.; Li, M.; Lu, Z.; Zhang, B. Tailoring desolvation kinetics enables stable zinc metal anodes. *J. Mater. Chem. A* **2020**, *8*, 19367–19374. [[CrossRef](#)]
64. Chen, Z.; Chen, H.; Che, Y.; Cheng, L.; Zhang, H.; Chen, J.; Xie, F.; Wang, N.; Jin, Y.; Meng, H. Arginine Cations Inhibiting Charge Accumulation of Dendrites and Boosting Zn Metal Reversibility in Aqueous Rechargeable Batteries. *ACS Sustain. Chem. Eng.* **2021**, *9*, 6855–6863. [[CrossRef](#)]

65. Wang, N.; Zhai, S.; Ma, Y.; Tan, X.; Jiang, K.; Zhong, W.; Zhang, W.; Chen, N.; Chen, W.; Li, S.; et al. Tridentate citrate chelation towards stable fiber zinc-polypyrrole battery with hybrid mechanism. *Energy Storage Mater.* **2021**, *43*, 585–594. [[CrossRef](#)]
66. Zhao, K.; Liu, F.; Fan, G.; Liu, J.; Yu, M.; Yan, Z.; Zhang, N.; Cheng, F. Stabilizing Zinc Electrodes with a Vanillin Additive in Mild Aqueous Electrolytes. *ACS Appl. Mater. Interfaces* **2021**, *13*, 47650–47658. [[CrossRef](#)] [[PubMed](#)]
67. Zhang, Y.; Zhu, M.; Wu, K.; Yu, F.; Wang, G.; Xu, G.; Wu, M.; Liu, H.; Dou, S.; Wu, C. An in-depth insight of a highly reversible and dendrite-free Zn metal anode in a hybrid electrolyte. *J. Mater. Chem. A* **2021**, *9*, 4253–4261. [[CrossRef](#)]
68. Gou, Q.; Luo, H.; Zhang, Q.; Deng, J.; Zhao, R.; Odunmbaku, O.; Wang, L.; Li, L.; Zheng, Y.; Li, J.; et al. Electrolyte Regulation of Bio-Inspired Zincophilic Additive toward High-Performance Dendrite-Free Aqueous Zinc-Ion Batteries. *Small* **2023**, *19*, 2207502. [[CrossRef](#)]
69. Ji, H.; Han, Z.; Lin, Y.; Yu, B.; Wu, D.; Zhao, L.; Wang, M.; Chen, J.; Ma, Z.; Guo, B.; et al. Stabilizing zinc anode for high-performance aqueous zinc ion batteries via employing a novel inositol additive. *J. Alloys Compd.* **2022**, *914*, 165231. [[CrossRef](#)]
70. Cao, H.; Huang, X.; Liu, Y.; Hu, Q.; Zheng, Q.; Huo, Y.; Xie, F.; Zhao, J.; Lin, D. An efficient electrolyte additive of tetramethylammonium sulfate hydrate for Dendritic-Free zinc anode for aqueous Zinc-ion batteries. *J. Colloid Interface Sci.* **2022**, *627*, 367–374. [[CrossRef](#)]
71. Liu, Z.; Wang, R.; Ma, Q.; Wan, J.; Zhang, S.; Zhang, L.; Li, H.; Luo, Q.; Wu, J.; Zhou, T.; et al. A Dual-Functional Organic Electrolyte Additive with Regulating Suitable Overpotential for Building Highly Reversible Aqueous Zinc Ion Batteries. *Adv. Funct. Mater.* **2023**, *34*, 2214538. [[CrossRef](#)]

**Disclaimer/Publisher's Note:** The statements, opinions and data contained in all publications are solely those of the individual author(s) and contributor(s) and not of MDPI and/or the editor(s). MDPI and/or the editor(s) disclaim responsibility for any injury to people or property resulting from any ideas, methods, instructions or products referred to in the content.